Front. Struct. Civ. Eng. 2023, 17(2): 205–223
https://doi.org/10.1007/s11709-022-0909-y

RESEARCH ARTICLE

Machine learning-based seismic assessment of framed structures with soil-structure interaction

Mohamed NOURELDIN, Tabish ALI, Jinkoo KIM*

Department of Global Smart City, Sungkyunkwan University, Suwon 16419, Korea
**Corresponding author. E-mail: jkim12@skku.edu*

ABSTRACT The objective of the current study is to propose an expert system framework based on a supervised machine learning technique (MLT) to predict the seismic performance of low- to mid-rise frame structures considering soil-structure interaction (SSI). The methodology of the framework is based on examining different MLTs to obtain the highest possible accuracy for prediction. Within the MLT, a sensitivity analysis was conducted on the main SSI parameters to select the most effective input parameters. Multiple limit state criteria were used for the seismic evaluation within the process. A new global seismic assessment ratio was introduced that considers both serviceability and strength aspects by utilizing three different engineering demand parameters (EDPs). The proposed framework is novel because it enables the designer to seismically assess the structure, while simultaneously considering different EDPs and multiple limit states. Moreover, the framework provides recommendations for building component design based on the newly introduced global seismic assessment ratio, which considers different levels of seismic hazards. The proposed framework was validated through comparison using non-linear time history (NLTH) analysis. The results show that the proposed framework provides more accurate results than conventional methods. Finally, the generalization potential of the proposed framework was tested by investigating two different types of structural irregularities, namely, stiffness and mass irregularities. The results from the framework were in good agreement with the NLTH analysis results for the selected case studies, and peak ground acceleration (*PGA*) was found to be the most influential input parameter in the assessment process for the case study models investigated. The proposed framework shows high generalization potential for low- to mid-rise structures.

KEYWORDS seismic hazard, artificial neural network, soil-structure interaction, seismic analysis

1 Introduction

Major earthquakes, such as the Mexico City (magnitude, *Mw* = 8.1, 1985) and Puebla (*Mw* = 7.1, 2017) earthquakes, highlighted the complex problem of soil-structure interaction (SSI) in urban areas [1] as well as the lack of comprehensive seismic performance assessment procedures. The multi-objective nature of the engineering design process for next-generation performance-based seismic design (PBSD) (e.g., [2,3]) requires multi-level seismic design criteria (e.g., operational, fully operational, life safety, etc.). To reduce the huge computational demand of PBSD, more soft computing application studies are needed in structural [4] and earthquake engineering [5]. Falcone et al. [6] noted that soft-computing techniques, such as neural networks, are emerging trends in seismic engineering, and more studies are needed in this research area. There has been little advancement in the development of an expert system related to the seismic evaluation of buildings [7] since early studies were conducted in 2005 (e.g., [8,9]). Therefore, it is essential to move research in this area forward by proposing expert system frameworks and new soft computing techniques related to seismic performance evaluation.

The inclusion of SSI in the analysis of structures resting on soft soils is important for the seismic assessment of structures. Buildings resting on soft soils may experience higher seismic demands if SSI is considered compared with fixed-base buildings [10]. van Nguyen et al. [11]

Article history: Received Jul 16, 2022; Accepted Sep 7, 2022

showed that SSI has a significant impact on the responses of nuclear reactors subjected to seismic excitations. Dao and Ryan [12] showed that SSI can amplify story drifts and accelerations in buildings isolated by friction bearings when the model is subjected to seismic shaking. Fatahi et al. [13] found that SSI can change the performance level of structures from life-safe to near-collapse.

Many studies have investigated the seismic demands of structures considering SSI using conventional methods. For example, Tang and Zang [14] investigated the effect of SSI on typical slender shear wall buildings by considering uncertainties using the maximum interstory drift (MIDR) as the main EDP. Fatahi et al. [13] and Reza Tabatabaiefar et al. [15] used the same EDP to investigate the effect of the SSI on moment-resisting building frames with different soil deposits. Recent studies, whether experimental or numerical, have relied primarily on using one EDP for seismic evaluation, such as MIDR (e.g., [16,17]) and base shear (e.g., [18]). However, these studies did not consider that multiple EDPs are required for serviceability and safety simultaneously.

Recent studies have highlighted the capability of soft computing to predict structural response, and some of these studies included SSI. For example, Khatibinia et al. [19] used a wavelet weighted least squares support vector machine to assess seismic reliability of RC structures including SSI. Farfani et al. [20] used data-based methods to produce additional experimental data for the seismic analysis of soil-pile-structure (SPS) systems. Mirhosseini [21] used support vector regression (SVR) to predict the seismic response of building systems considering the SSI effects. Sharma et al. [10] developed an ANN to predict the natural period of RC building frames supported on pile foundations for various soil types. Other studies have attempted to predict building response without considering SSI using different machine learning techniques (MLTs), such as supervised and unsupervised learning algorithms (e.g., [22]), ANN (e.g., [23–27]), and convolutional neural networks (e.g., [28]). These studies attempted to introduce soft computing techniques as an alternative to conventional methods for predicting building response; however, they did not provide a comprehensive framework for the seismic assessment of structures.

Conventional inelastic design procedures excluding SSI are deemed inadequate for guaranteeing the structural safety of building frames resting on soft soil deposits [13]. Other studies have shown that conventional methods that consider SSI in estimating structural responses (e.g., [2]) are conservative in many cases [29] or unsafe (or uneconomic) in other cases [30,31]. In addition, these methods are suitable only for regular structures. Most studies are highly concerned with structural safety (i.e., story drift [32]), and few studies (e.g., [33]) consider serviceability, which is found to be crucial for important facilities such as hospitals and data centers [34]. Floor acceleration is commonly used as a representative engineering demand parameter (EDP) for serviceability [35].

Another important aspect that is commonly overlooked, especially in retrofitting and optimization studies, is the increase in the seismic base shear demands on the foundation due to global retrofitting (e.g., attachment of energy dissipating devices) [36–39]. This necessitates the inclusion of base shear (V) as an additional EDP during the early design stage or seismic assessment process. In addition, next-generation PBSD [2] requires multiple EDPs (e.g., story-drift, floor acceleration) to make the seismic fragility groups required for the assessment and performance-based design of buildings. Moreover, recent seismic evaluation and retrofit standards (e.g., [40]) require consideration of different limit states (e.g., immediate occupancy, life safety, collapse prevention) in the seismic assessment process. Another important aspect that must be included in conventional seismic assessment procedures are seismic-enhancement predictions (or retrofitting), required to meet a given seismic performance level.

Soft computing techniques are gaining momentum for solving complicated engineering problems, such as crack propagation prediction [41], damage assessment in FGM composite plates [42], fast tracking for structured light measurement [43], damage identification in plate structures [44], and structural damage detection [45]. This makes soft computing techniques appealing tools for solving complicated seismic engineering problems considering SSI.

Based on the previous discussion, it can be concluded that there is a great need for a comprehensive expert system for seismic performance assessment that considers different input variables related to the structure, SSI, and earthquake events. The main motivation of the current research is attributed to the lack of an automated seismic assessment framework that considers different EDPs, as well as multiple limit state criteria (such as life safety and collapse prevention limit states) considering SSI. Moreover, there is a need for a global assessment index that provides the building engineer with an easy and simple metric to judge the performance of any component in the building at different hazard levels (such as design-level earthquakes and maximum-considered earthquakes). This is considered a highly needed design approach recommended by modern seismic guidelines and codes (e.g., [2,40]), and more research is needed to fill this gap, especially for studies considering SSI.

In the current study, an expert system framework is developed based on supervised MLTs and is used for predicting the seismic performance of low- to mid-rise frame building structures considering SSI. The proposed framework considers both safety (maximum interstory drift ratio, D, and base shear, V) and serviceability (floor

acceleration, A) in the seismic performance assessment. The framework can be adjusted to the important input parameters for which the EDPs are sensitive. A new global seismic assessment ratio is introduced that accounts for the combined effect of three different EDPs (D, A, and V). In addition, the proposed framework allows the designer to assign different weight factors to the preferred EDPs to reflect the importance of a particular EDP for a specific limit state or building condition. Conventional methods considering SSI (e.g., [29]) are used for comparison, and an NLTH analysis is used to verify the proposed framework results. The proposed procedure provides an expert opinion regarding the structural seismic performance considering the variability in the SSI, structural characteristics, and ground motion input.

2 Proposed framework

As shown in Fig. 1, the proposed expert system framework consists of three main parts: dataset preparation and processing, MLT selection, and seismic performance evaluation. The main input for the framework is related to the structure, earthquake, and SSI information. The output is the seismic performance classification of the structure and the required seismic retrofit. The framework can be summarized as follows.

Steps related to data-set preparation and processing.

1) A dataset related to framed structural systems (three to ten stories) was prepared. Structural models are selected such that they represent the common prototype building structures under investigation. Earthquake records and response spectra were prepared considering

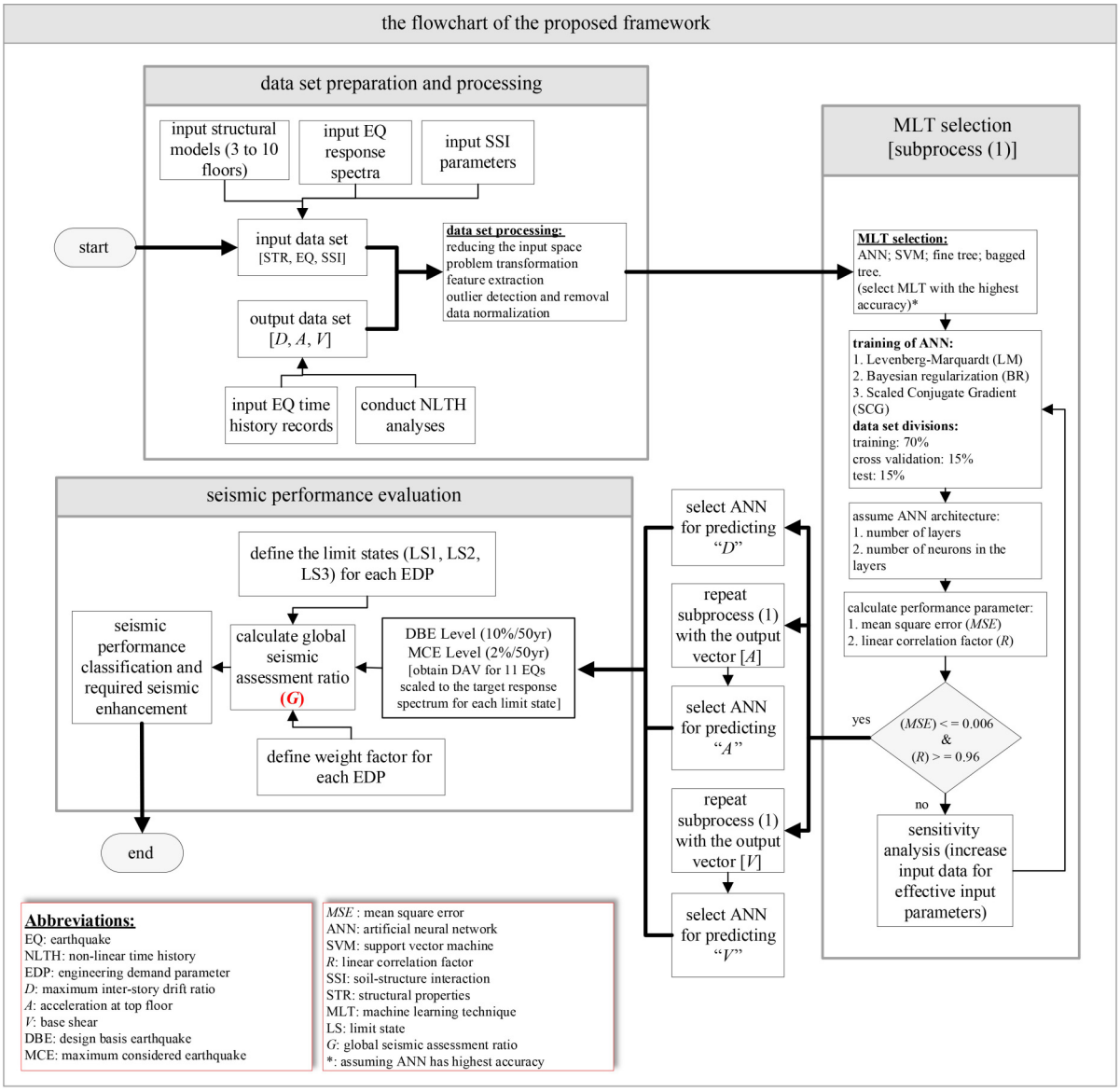

Fig. 1 Flowchart of the proposed framework.

the variability of earthquake characteristics. The main SSI variables affecting the seismic response were selected, and a reasonable range based on previous studies was used for each variable. In the current study, the soil elastic modulus, E, and Poisson's ratio, μ, were considered representative of the other soil model variables, such as the shear modulus, G, and shear velocity, V_s, to reduce the input space of the framework.

2) Non-linear time history analyses (NLTHAs) were conducted by considering the soil continuum around the foundation and earthquake records. An algorithm coded in OpenSees [46] and MATLAB [47] environments was used to conduct NLTHAs and obtain D, A, and V.

3) The dataset input vector was [number of stories, earthquake response spectrum, and SSI parameters] and the output vector was [D, A, V]. Data processing, such as outlier detection and removal, data normalization, and input space reduction was conducted on the original data to enhance the performance of the MLT in the next step.

Steps related to MLT selection.

4) Different MLTs were investigated (e.g., ANN, SVM, fine tree, and bagged tree) to achieve the highest accuracy required. Subsequently, the optimum hyperparameters of the selected MLT were fine-tuned, and the best optimization algorithm was used for training. For example, if an ANN is selected, different back-propagation optimization algorithms to update the weight and bias values are investigated (e.g., Levenberg−Marquardt (LM), Bayesian regularization (BR), and Scaled Conjugate Gradient (SCG)) to obtain the optimum performance in terms of accuracy and time. The procedure assumes that ANN provides the highest accuracy compared with other MLTs.

5) To avoid overfitting, the dataset was divided into training (70%), validation (15%), and testing (15%). Different ANN architectures, including the number of layers and neurons in each layer, were checked for the best performance.

6) Mean square error (*MSE*) and linear correlation factor (R) were used to assess the performance of the selected MLT. The minimum acceptance criterion was used to maintain the required accuracy of the selected MLT. If this criterion was exceeded, a sensitivity analysis was conducted to check the most important input variables and increase their representation in the original dataset. This process was repeated until the prescribed acceptance criteria were met. To maintain the highest accuracy, each EDP was predicted using an individual MLT. The minimum acceptance criteria were arbitrarily chosen to maintain the preferred level of accuracy required by the designer. Because the minimum criteria is highly related to the availability of a huge dataset, it can be relaxed if the available dataset is not numerous.

Steps related to seismic performance evaluation.

7) At least two different levels of seismic hazard should be defined (e.g., 10% and 2% probability of exceedance in 50 years), which can be mapped onto the design basis earthquake (DBE) and maximum considered earthquake (MCE). Earthquake records based on these hazard levels can be used to obtain DAV values.

8) The limit states (e.g., immediate occupancy (IO), life safety (LS), and collapse prevention (CP)) for each EDP should be defined. The weight of each EDP should be defined by considering the importance of the EDP on the seismic response of the structure.

9) A global seismic assessment ratio (G) is calculated as follows:

$$G = 1 - \left(F_{\mathrm{d}} \frac{D_{\mathrm{avg}}}{D_{\mathrm{lim}}} + F_{\mathrm{A}} \frac{A_{\mathrm{avg}}}{A_{\mathrm{lim}}} + F_{\mathrm{V}} \frac{V_{\mathrm{avg}}}{V_{\mathrm{lim}}} \right) \leqslant 1.0, \tag{1}$$

where D_{avg}, A_{avg}, and V_{avg} are the averages of D, A, and V, respectively, obtained from the set of earthquakes corresponding to each hazard level; D_{lim}, A_{lim}, and V_{lim} are the limits corresponding to each EDP for a specific limit state. Each EDP ratio $\left(\frac{D_{\mathrm{avg}}}{D_{\mathrm{lim}}} \,\&\, \frac{A_{\mathrm{avg}}}{A_{\mathrm{lim}}} \,\&\, \frac{V_{\mathrm{avg}}}{V_{\mathrm{lim}}} \right)$ should be less than 1.0. F_{D}, F_{A}, and F_{V} are the weight factors of D, A, and V, respectively. These weight factors should range between 0 and 1.0 (values near 1.0 have more impact on the seismic response evaluation) according to the designer's preference, and the following condition should be satisfied.

$$F_{\mathrm{d}} + F_{\mathrm{A}} + F_{\mathrm{V}} = 1.0. \tag{2}$$

10) Finally, a seismic performance classification based on the G value was established. In the current study, the assumed classes good, moderate, poor, and not acceptable were mapped to G values of ($1.0 > G \geqslant 0.75$), ($0.75 > G \geqslant 0.45$), ($0.45 > G \geqslant 0.2$), and ($0.2 > G$), respectively.

3 Modeling of soil structure and ground motions

In this section, the case study structures, SSI modeling, and ground motion records are presented for analysis.

3.1 Building model

Because the effect of the building height on the structural natural period is more important than its width [10], different frame models in terms of the number of floors were used for the dataset input. The structural models were selected such that they represent common prototype frame buildings with three bays (span and story height are shown in Fig. 2). Similar archetype models have been used in FEMA-P695 [48]. The plan and elevation of one of the models are shown in the Fig. 2. For analysis, the use of a 2D frame is permitted because no torsional

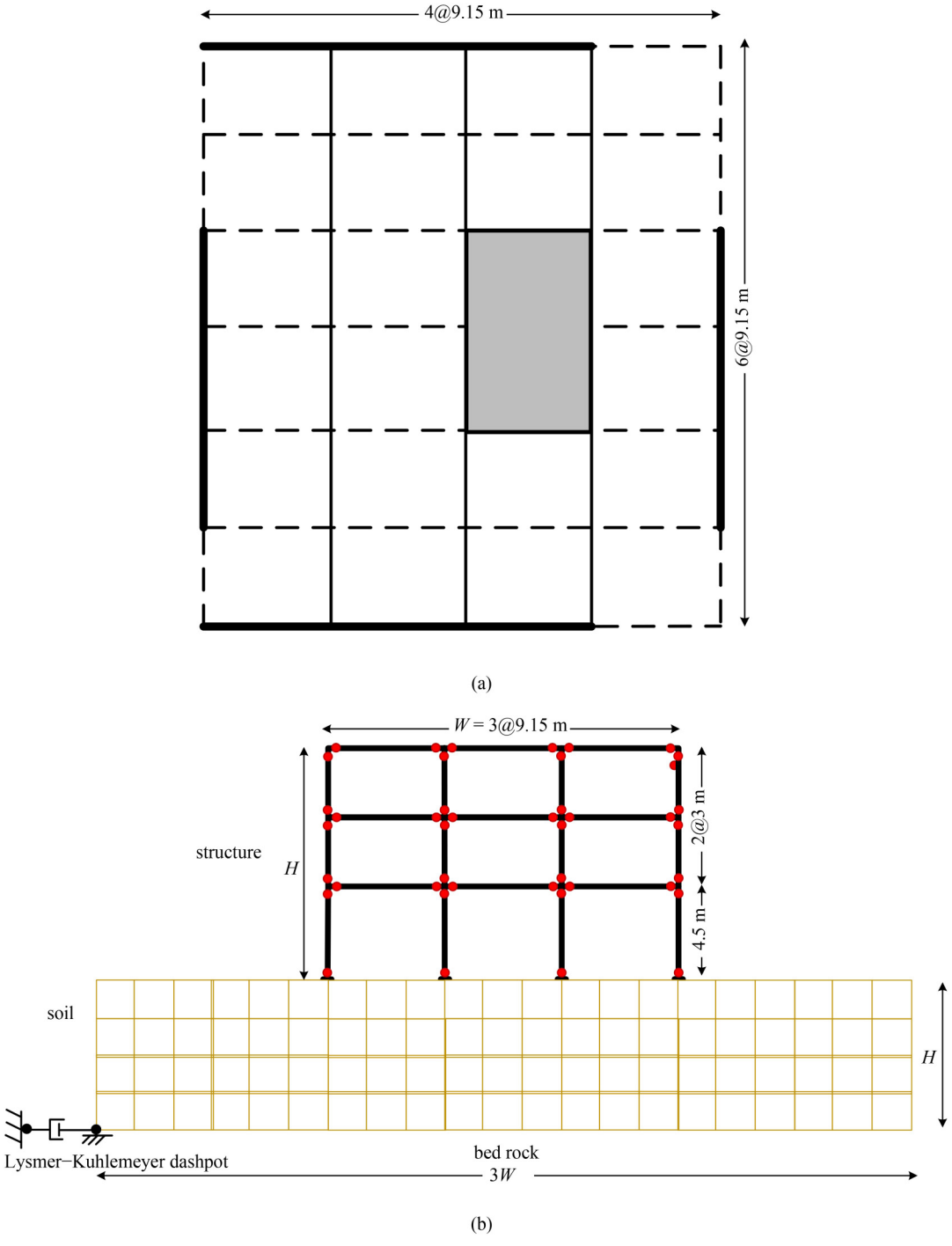

Fig. 2 Configuration of the analysis model frames: (a) plan view; (b) 3-story frame elevation with SSI Model.

behavior is expected in the building [40]. The building was designed for a dead load of 4.1 kN/m^2 and a live load of 2.5 kN/m^2. Table 1 lists the section properties of the steel elements (nominal yield strength of 345 MPa) used for the training models. Three-, five-, and nine-story models were used for training. The columns and beams of the structures were modeled as beam-column elements using the element library built in the OpenSees software [46]. The connections between the columns and beams were modeled using a zero-length element. There are different methods for crack modeling [49–55], in which the modified Ibarra−Krawinkler deterioration model [56] was used for modeling the non-linear force-deformation relationship of the zero-elements.

3.2 Soil-structure interaction model

SSI modeling can be broadly categorized into two types. The first approach, which is more accurate, is the direct approach, in which the soil continuum around the

foundation is modeled using the finite-element method (FEM). The second approach, which is less accurate, is referred to as the simplified approach, in which the surrounding soil is modeled with a series of springs and dashpots. The first approach was used in this study. The width of the soil domain was thrice the width of the building, and the depth was equal to the height of the building. Isoperimetric four-node quadrilateral finite elements with two degrees of freedom per node were used to model the soil region, considering the plain strain conditions. Joints at the soil-structure interface were modeled to have the same degree of freedom. The radiation damping of the soil was considered by Lysmer–Kuhlemeyer dashpots [57]. A typical soil damping ratio of 5% was used [58]. To represent the soil parameters in the MLT training phase, a range of elastic moduli (E) and Poisson's ratios (γ) were used. For the elastic modulus E, the range was 478–210000 kN/m^2, divided into three divisions. For γ, the range was 0.2 to 0.45, divided into four divisions [59].

3.3 Ground motions

The ground motions are represented by the peak ground accelerations (*PGA*s) and frequency contents (i.e., response spectrum), which capture the main characteristics of the ground motion excitations [60]. Training the MLT using the response spectra of earthquake events enhances the performance of the entire framework because nonlinear response prediction is highly affected by the frequency contents of the earthquake [61]. To introduce variability in the input ground motions used in the current study, 100 different real ground excitation events from the PEER [62] database were used. The ranges of the input parameters are listed in Table 2. The variations in these seismic excitations include *PGA*, magnitude (*Mw*), source-fault mechanism, site-to-source distance, shear velocity (V_{s30}), and the lowest useable frequency. More earthquake events are represented in the range of 0.3g to 0.6g as it is the practical range for the seismic design of buildings. Figure 3(a) shows the response spectra of the 100 input earthquakes, and Fig. 3(b) shows a histogram of the *PGA* ranges used. This selection guarantees the diversity of the input earthquakes over the expected range of occurrence.

To test the proposed framework's potential for seismic assessment, different seismic hazard levels were used, and the results were compared with widely accepted conventional methods and the NLTH analysis method; the latter is considered the reference method. The records used for these hazards were not used in training the MLT. Two seismic hazard levels of 10% and 2% probability of exceedance in 50 years (shortened 10/50 and 2/50, respectively) were used. These levels are equivalent to life safety and collapse prevention structural performance, respectively, for risk category II buildings to achieve a basic performance objective equivalent to new building standards [40]. The structural models were assumed to be located in California (LA-USA), with latitude and longitude coordinates of 34.0° and −118.2°, respectively. Figure 4 shows the response spectra of the 11 earthquake records and their arithmetic mean, along with the target response spectrum for each seismic hazard level. The 22 earthquake records (Table 3) were obtained from the PEER NGA Database [62].

Table 1 Section properties and element details of model structures

item	model	standard section
beams	3 and 5-story	W33 × 118
	9-story	W12 × 53
columns	3-story	(1−3 story) W14 × 257
	5-story	(1−2 story) W14 × 311
		(2−5 story) W14 × 257
	9-story	(1−2 story) W18 × 130
		(3−5 story) W14 × 90
		(6−7 story) W14 × 61
		(8−9 story) W14 × 48

4 Results and discussion

In this section, we discuss the performance and accuracy

Table 2 Parameters of input earthquake records

item	limit/ EQ name	*PGA* (*g*)	magnitude (*Mw*)	source to site distance (km)	V_{s30} (m/s)	lowest useable frequency (Hz)	source-fault mechanism
limits of parameters	upper	1.800	7.62	218.13	1428	3.750	normal; reverse: reverse oblique; strike slip
	lower	0.017	4.20	0.56	169.8	0.025	
earthquake samples*	"NW Calif-03"	0.301	5.80	53.73	219.3	0.500	strike slip
	"Cent. Calif-01"	0.340	5.30	25.81	198.7	0.375	strike slip
	"Parkfield"	0.370	6.19	63.34	493.5	0.625	strike slip
	"San Fernando"	0.579	6.61	22.77	316.4	0.100	reverse
	"San Fernando"	0.644	6.61	35.54	529.0	0.250	reverse

*Note: EQ records will be used for the 4th model.

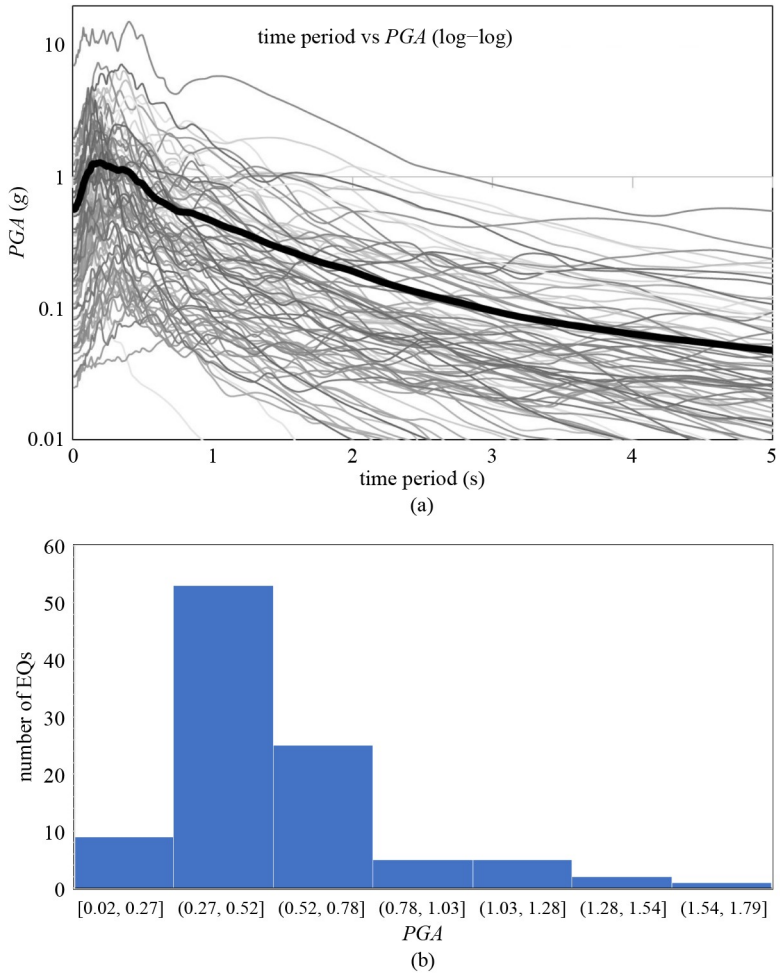

Fig. 3 Input earthquakes used for the framework: (a) response spectra of 100 input earthquakes; (b) histogram of the *PGA*.

of the proposed framework. Subsequently, the framework was validated using NLTH analyses and compared with conventional methods. The generalization potential of the framework was examined, and the global assessment ratio was estimated for all models. Finally, the results are discussed, showing the superiority of the proposed framework over conventional methods.

4.1 Enhancing the performance of the selected machine learning technique

The sensitivity of the EDPs to the input parameters was investigated to enhance the performance of the selected MLT. Based on the sensitivity analysis results, increasing the data input related to a particular input parameter may increase accuracy. A sensitivity analysis was conducted by calculating the mean (μ) and standard deviation (σ) of the input parameter values. Then, 100 variations of the input parameter were induced within the range of ($\mu \pm \sigma$), and the corresponding outputs were calculated using the MLT. The standard deviation (σ) of the output was calculated. A high standard deviation (σ) of the output parameter indicated a high sensitivity to the corresponding input parameter [20]. For example, in the case of the 3-story model, the sensitivity analysis showed that the three EDPs are most sensitive to *PGA*, as shown in Fig. 5. This requires an increase in the number of EQs used in the input dataset within a particular range. In the current study, the number of EQs increased with greater diversity in the *PGA* values in the range of 0.3*g* to 0.6*g*. It was found that the required accuracy criteria were satisfied after increasing the *PGA* input data in this range.

Another technique to enhance the accuracy of MLT can be achieved by removing unnecessary input parameters to reduce the input space. For example, SSI input parameters can be removed if they have a marginal effect on output results. The structure-to-soil stiffness ratio can be checked to determine the significance of SSI on seismic responses [63]:

$$\frac{h}{V_s T} > 0.1, \tag{3}$$

where h is the effective height of the structure, which is two-thirds of the building height; V_s is the average effective overburden-corrected shear wave velocity of the soil profile below the site; and T is the fixed-base period

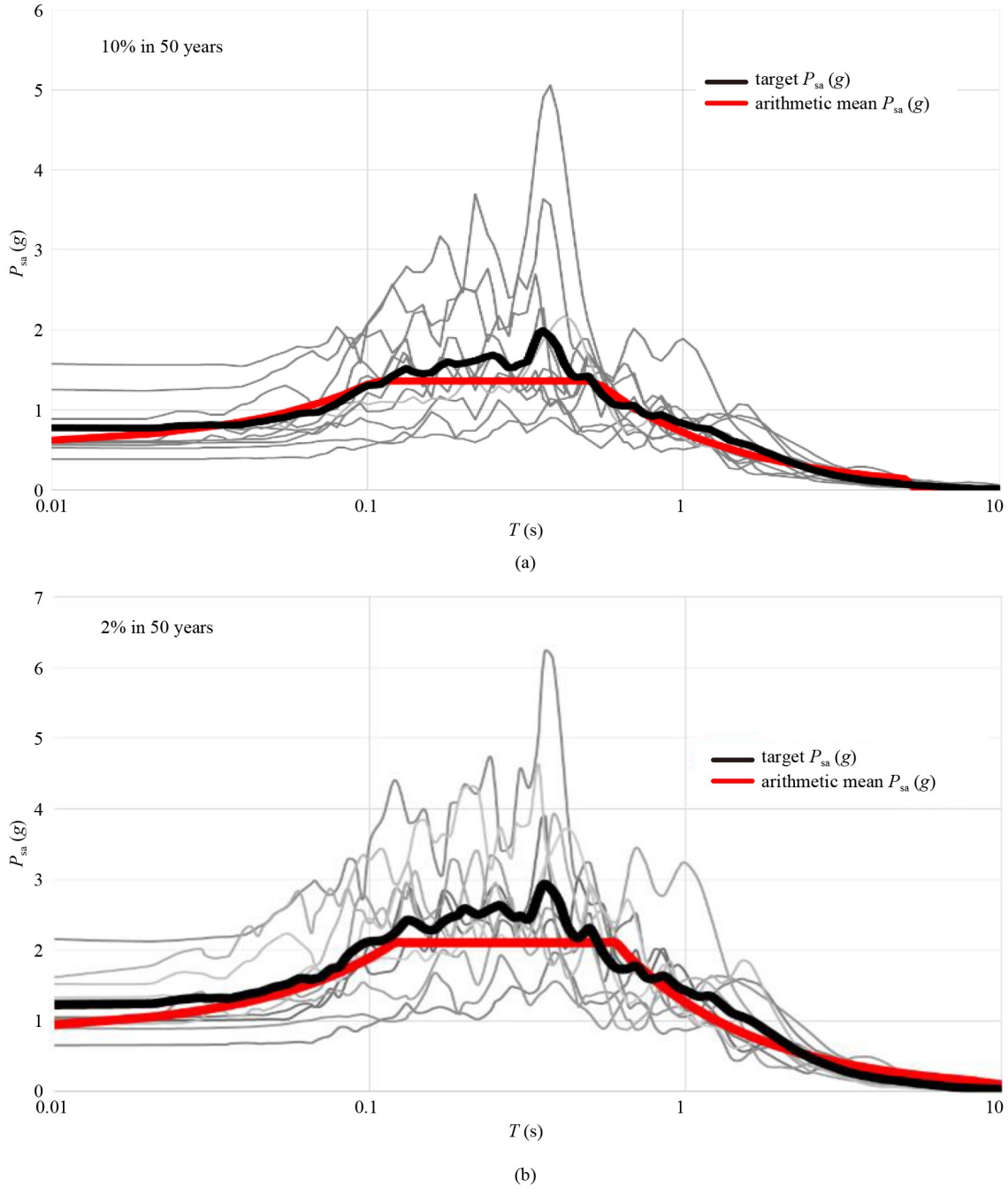

Fig. 4 Response spectra of the 11 earthquakes and the target spectrum for seismic hazards with probability of exceedance in 50 years of: (a) 10%; (b) 2%.

of the building in the direction under consideration. Values of $h/(V_sT)$ exceeding 0.1 indicate that the SSI effects are likely to be significant, which is the case for the models used in the current study.

To improve the prediction potential of MLT, data normalization is used to map the data to a uniform scale, especially if the data have widely different scales. A min-max linear transformation technique was used to scale all values within a range of 0–1. The following normalization equation was used [64]:

$$y_{new} = \left(\frac{y_{old} - min1}{max1 - min1}\right)(max2 - min2) + min2, \quad (4)$$

where y_{new} and y_{old} are the new and old values, respectively; $min1$ and $max1$ are the minimum and maximum values of the original data range, respectively; and $min2$ and $max2$ are the minimum and maximum values of the new data range, respectively. Figure 6 shows the normalized V of the 3-story frame for 1200 samples. The same was generated for outputs D and A (a total of 3600 outputs for each model).

Table 3 List of the earthquake records used in the nonlinear dynamic analyses

probability of exceedance in 50 years	sequence number	earthquake name	*PGA* (*g*)	magnitude	fault type	source distance (km)	scale factor
10%	1	"Imperial Valley-02"	0.59	6.95	strike slip	6.09	2.09
	2	"Kern County"	0.61	7.36	reverse	38.42	3.82
	3	"Northern Calif-03"	0.38	6.5	strike slip	26.72	2.33
	4	"Parkfield"	1.26	6.19	strike slip	9.58	2.76
	5	"Parkfield"	1.57	6.19	strike slip	15.96	4.34
	6	"Borrego Mtn"	0.52	6.63	strike slip	45.12	3.91
	7	"San Fernando"	0.60	6.61	reverse	22.77	2.57
	8	"San Fernando"	0.75	6.61	reverse	22.23	4.96
	9	"San Fernando"	0.57	6.61	reverse	24.16	4.98
	10	"Managua Nicaragua-1"	0.89	6.24	strike slip	3.51	2.38
	11	"Managua Nicaragua-2"	0.77	5.2	strike slip	4.33	2.94
2%	12	"Imperial Valley-02"	1.009	6.95	strike slip	6.09	3.5903
	13	"Kern County"	1.043	7.36	reverse	38.42	6.5615
	14	"Northern Calif-03"	0.655	6.5	strike slip	26.72	4.0082
	15	"Parkfield"	2.107	6.19	strike slip	9.58	4.7448
	16	"Borrego Mtn"	0.890	6.63	strike slip	45.12	6.7084
	17	"San Fernando"	0.993	6.61	reverse	22.77	4.4173
	18	"San Fernando"	1.289	6.61	reverse	22.23	8.5081
	19	"San Fernando"	1.586	6.61	reverse	0	1.2998
	20	"San Fernando"	0.958	6.61	reverse	24.16	8.5419
	21	"Managua Nicaragua-1"	1.522	6.24	strike slip	3.51	4.0902
	22	"Managua Nicaragua-2"	1.329	5.2	strike slip	4.33	5.0514

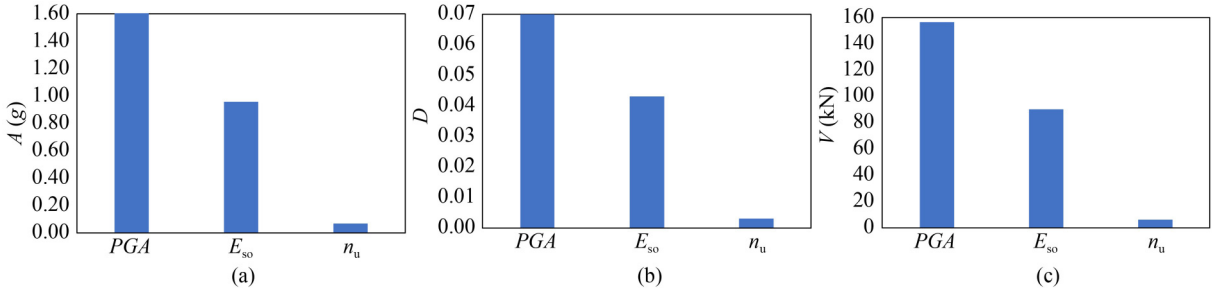

Fig. 5 Sensitivity of EDPs to *PGA*, elastic modulus (E_{so}), and Poisson's ratios (n_u): (a) *V*; (b) *D*; (c) *A*.

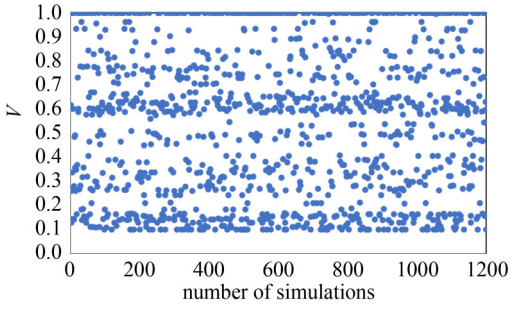

Fig. 6 Normalized *V* in the 3-story building (1200 samples).

4.2 Accuracy of the machine learning technique

Different MLTs were investigated to obtain the highest possible accuracy. Figure 7 shows the accuracy of different MLTs (SVM, bagged tree, fine tree, and ANN) for the 3-story model, where ANN was found to provide the highest accuracy in terms of the *MSE*. Different algorithms, topologies, and activation functions were studied to select the ANN with the highest possible accuracy. Figure 8 shows the effect of three training backpropagation algorithms (SCG, Levenberg−Marquardt (LM), and Bayesian Regulation (BR)) on the accuracy of

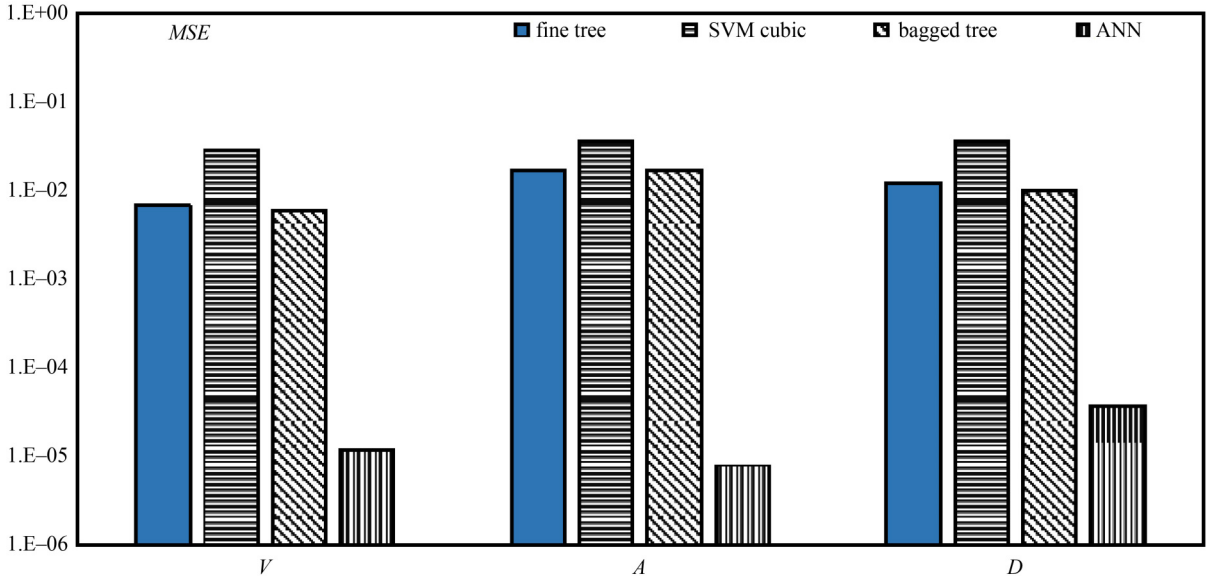

Fig. 7 Accuracy of different MLTs for the output EDPs.

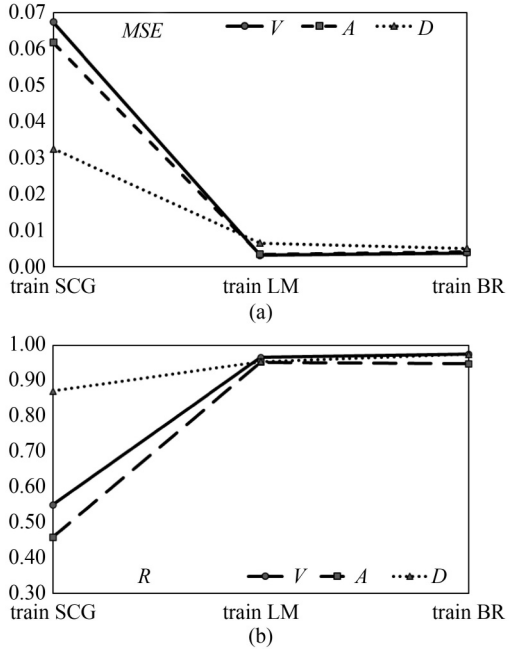

Fig. 8 Effect of training algorithm on: (a) *MSE*; (b) *R*.

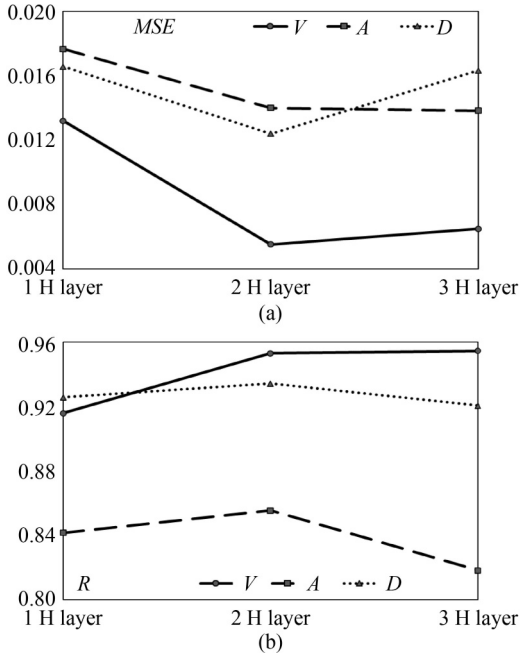

Fig. 9 Effect of number of hidden layers on: (a) *MSE*; (b) *R*.

the ANN. It can be observed that the LM and BR algorithms obtained higher accuracies than the SCG algorithm for the three EDPs. It should be noted that *D* is less sensitive to the training algorithms than *V* and *A*. Figure 9 shows the effect of the number of hidden layers on the accuracy of the ANN, where two hidden layers provided the highest accuracy for all EDPs. Figure 10 shows the effect of the number of neurons on accuracy. It was found that the use of 10 neurons provided the least mean square error; conversely, 20 neurons provide a slight edge over 10 neurons based on the *R* values for *V* and *D*.

Figure 11 shows the effect of the activation function, where it can be observed that the hyperbolic tangent sigmoid (TANSIG) function provides the most accurate results compared with the log sigmoid transfer (LOGSIG) and linear transfer (PURLIN) functions. Based on this, the best accuracy can be achieved by using an ANN with two layers, the TANSIG activation function, the LM training algorithm, and 10 neurons per layer. Figure 12 shows an example of the *R* plot and the error histogram for *V* and *D* after using the optimum parameters of the ANN for the 3-, 5-, and 9-story models.

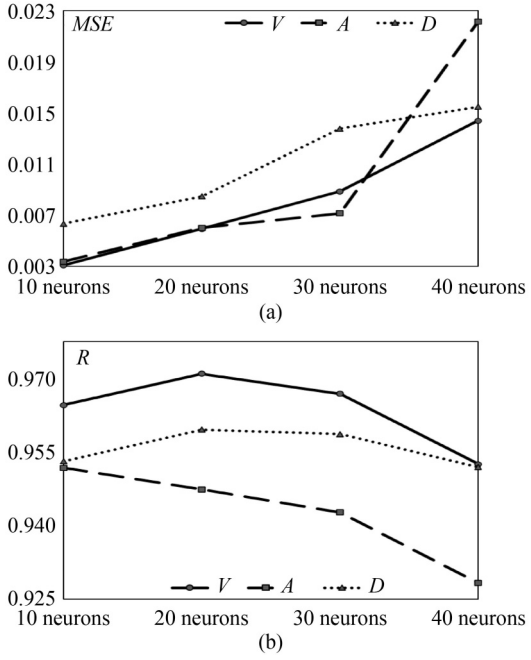

Fig. 10 Effect of number of neurons on: (a) *MSE*; (b) *R*.

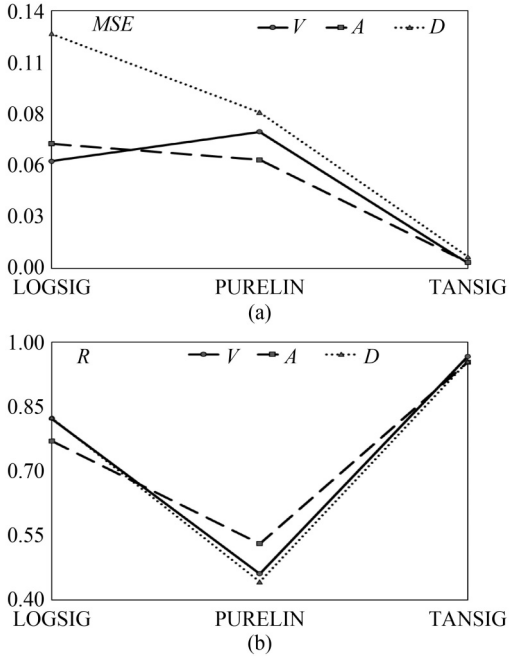

Fig. 11 Effect of activation function on: (a) *MSE*; (b) *R*.

4.3 Validation using non-linear time history analyses and comparison with ASCE methods

To validate the proposed framework, the MLT results were compared with those of the NLTH analysis using 22 earthquakes representing design-level earthquake (DLE) and maximum considered earthquake (MCE), as described in Section 3. Figure 13 shows the comparison results (for *V*, *A*, and *D*), where ANN represents the MLT; and FEM represents the NLTH analysis using the FEM method. The results indicate that there is very good agreement between the results of the proposed framework and NLTH analysis for both the DBE and MCE levels.

The proposed framework results were compared with those of conventional methods for calculating seismic responses including SSI. FEM using an NLTH analysis was used as a reference in this comparison. One of the most common methods used for calculating the seismic base shear with SSI is the ASCE [29] method.

Figure 14 shows the analysis results for the DBE and MCE levels of the ASCE methods (fixed, ELFP, and NLP), two different MLTs (ANN and bagged tree), and the NLTH analysis method. In this figure, the ASCE method using the equivalent lateral force procedure with SSI is denoted as ELFP. For comparison purposes, two other ASCE methods were used: the fixed base procedure, Fixed, and the nonlinear procedure to account for the kinematic SSI effect on the ground motion input, NLP. The proposed framework is denoted as ANN, and for comparison purposes, the bagged tree technique is included. The FEM using an NLTH analysis is denoted as FEM in the figure (reference method). The figure shows that the proposed framework with ANN provides the most accurate results compared with the ASCE methods.

For example, in the case of *V*, ELFP overestimated the results by 12.53% and 11.89% for the DBE and MCE levels, respectively. In the Fixed case, these values increased to 17.68% and 17.01%, respectively; and in the NLP case, they increased to 16.31% and 16.49%, respectively. However, in the ANN case, the difference was reduced to 7.75% and 0.96% for the DBE and MCE levels, respectively. In the case of *D*, the ELFP overestimated the results by 10.94% and 4.54%, respectively. Other ASCE methods show more conservative results than the ELFP. However, the difference in the case of the ANN was reduced to 2.34% and 1.23% for the DBE and MCE levels, respectively. This shows that the proposed framework provides a higher accuracy in predicting *V* and *D* compared with conventional ASCE methods. It was found that the bagged tree technique underestimates the response values in general, especially in the case of *D*, as can be observed in Fig. 14(b).

4.4 Generalization of the framework

The generalization potential of the proposed framework was tested by investigating two irregularities: stiffness and mass irregularities. Figure 15 shows the 3-story model with mass irregularity on the second floor owing to the addition of heavyweight equipment. The same figure shows the 4-story model with a vertical irregularity (soft story) in the first story, according to ASCE-7 [29]. The cross-sections of the first- and second-story columns of

the 4-story model are W14 × 311, and those of the third- and fourth-story columns are W14 × 257. All beams were designed with W14 × 118 sections. This model was not used in the training process of the MLT. For the 3-story model, the same modeling of the elements used in Section 3 was applied. The earthquake records (indicated with an asterisk in Table 2) used for NLTH analyses were not used in the training process of the framework.

Figure 16 shows the results of the mass-irregular 3-story model using an NLTH analysis and the proposed

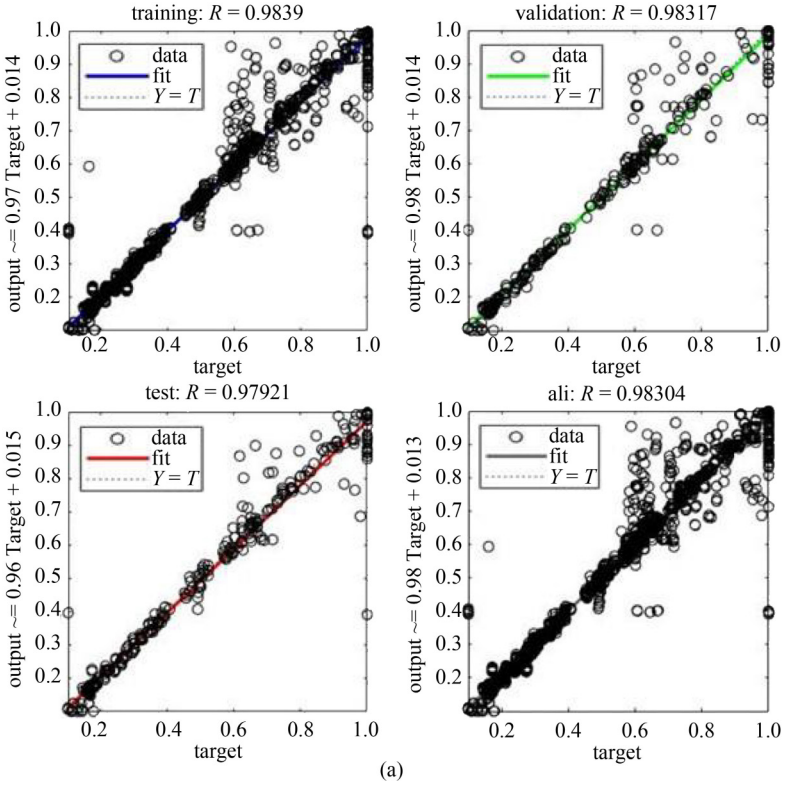

(a)

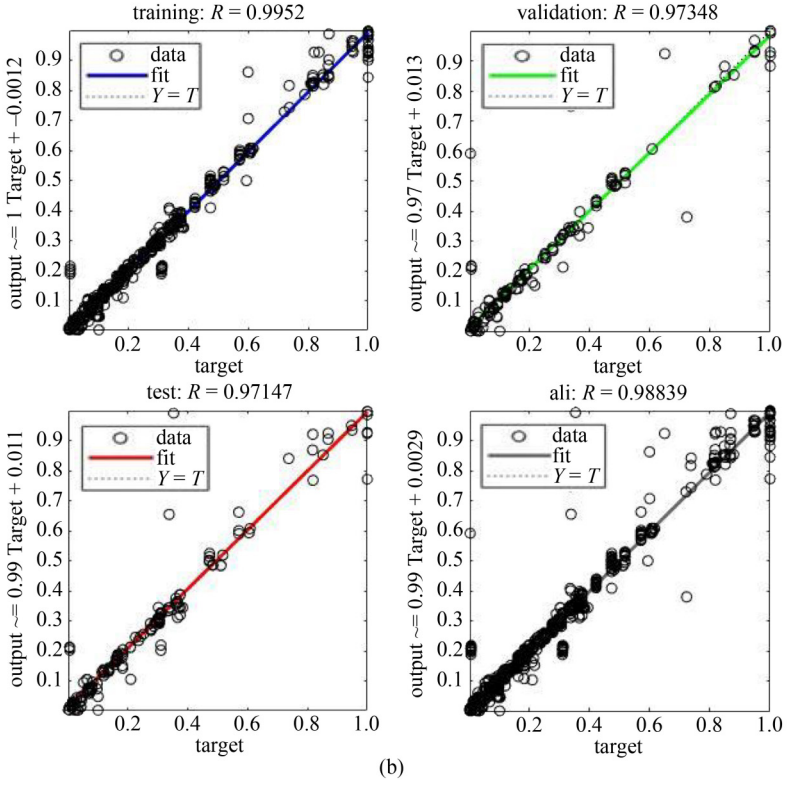

(b)

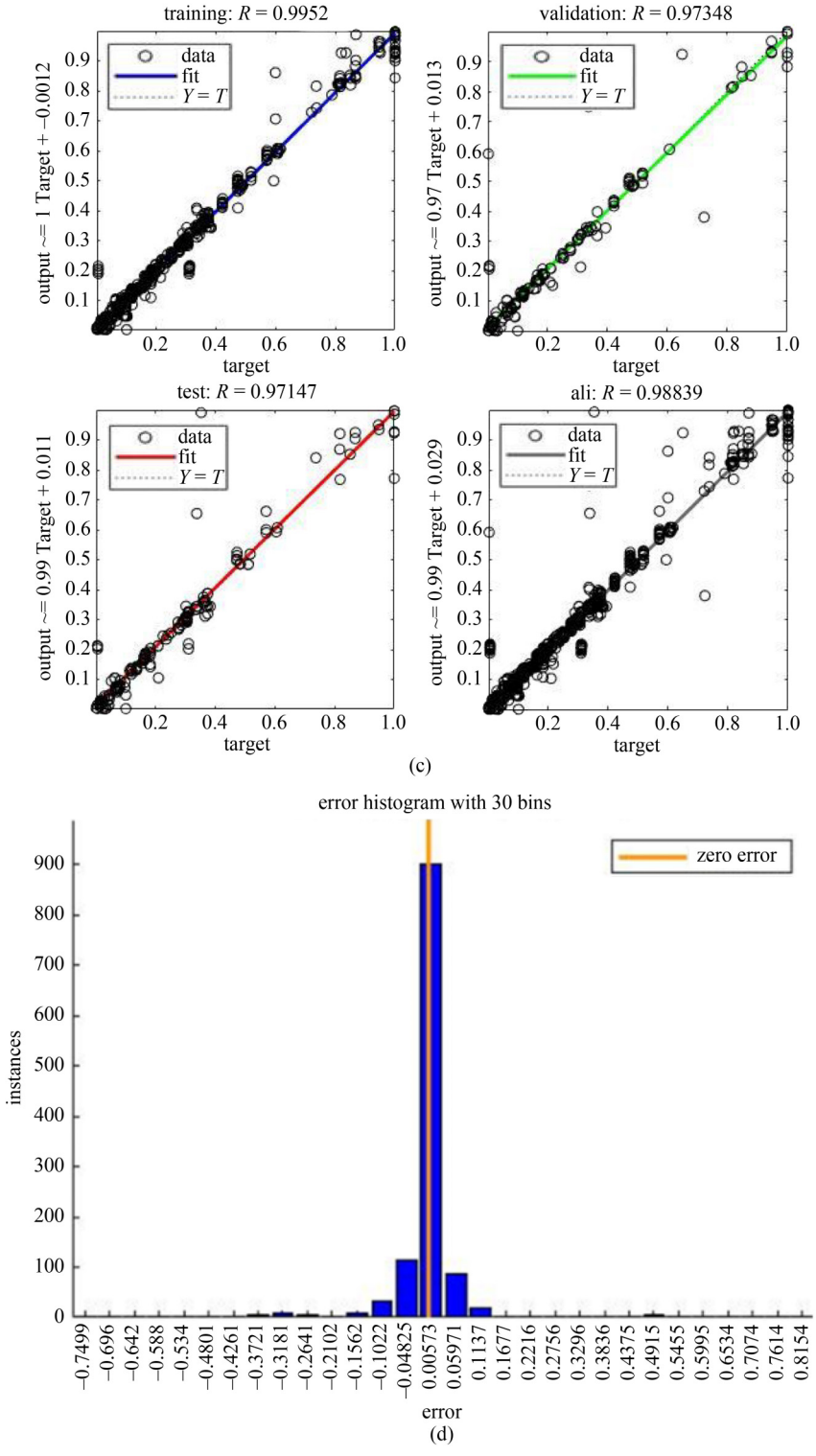

Fig. 12 Accuracy of the ANN in the example structures: (a) *R* plot of *V* in 3-story model; (b) *R* plot of *V* in 5-story model; (c) *R* plot of *V* in 9-story model; (d) error histogram of *D*.

MLT (ANN) for the DBE and MCE levels. For the majority of earthquakes, the results from both the methods were almost identical. For the DBE level, the difference in averages of the 11 EQs results using the proposed MLT and NLTH methods for *V*, *A*, and *D* were 6.9%, 5.5%, and 1.5%, respectively. For the MCE level, the values were 1.1%, 0.99%, and 5.7%, respectively.

Figure 17 shows the results of the stiffness-irregular 4-story model using an NLTH analysis and the proposed MLT (ANN) for five different earthquakes to test the

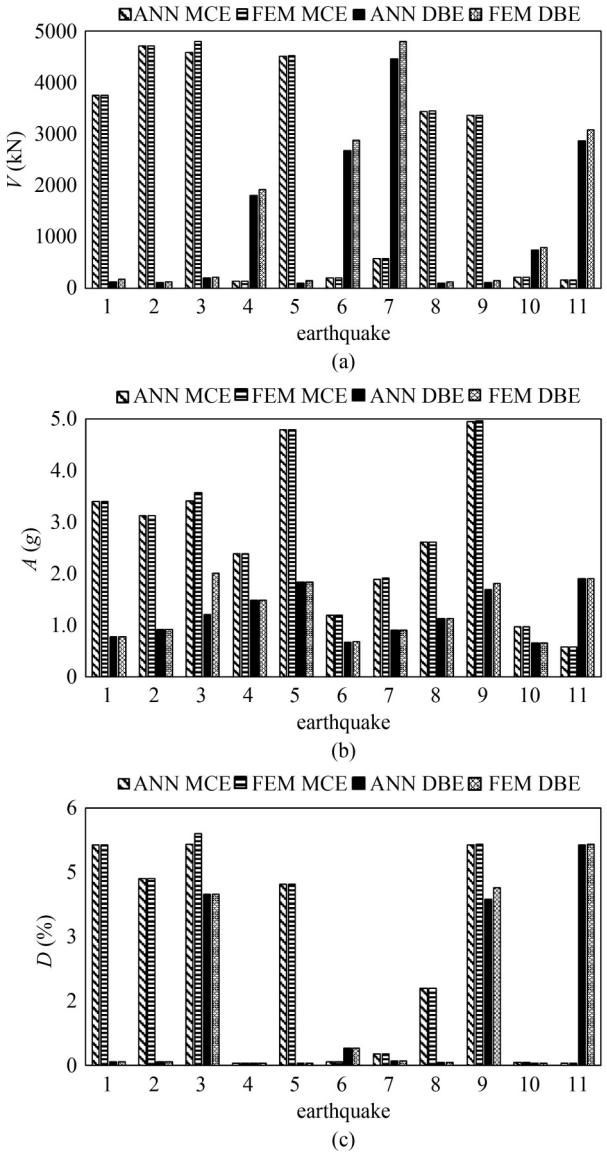

Fig. 13 Validation of the MLT results using NLTH analysis results: (a) V; (b) A; (c) D.

validity of the proposed MLT. These earthquakes were not used in the training phase, and their characteristics are listed in Table 2. The MLT results are in good agreement with those obtained from the NLTH method. The differences between the results of the five EQs obtained from the proposed MLT and the NLTH method for V, A, and D were 0.001%, 3.09%, and 0.05%, respectively.

4.5 Global seismic assessment ratio

The seismic assessment was evaluated using the proposed framework for regular 3-story, mass-irregular 3-story, and stuffiness-irregular 4-story models. Table 4 lists the details of the global seismic assessment ratio (G) estimation for the previous models.

For the regular 3-story model, the same value of 1/3

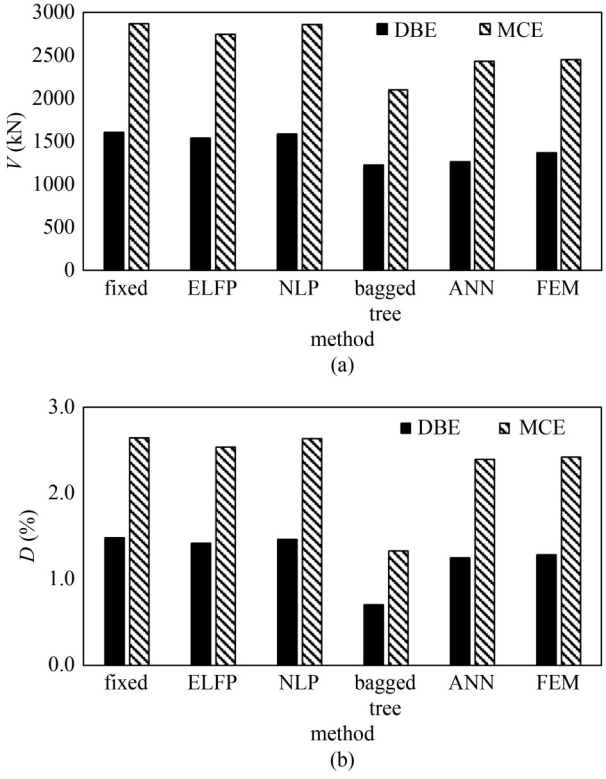

Fig. 14 Comparison of the MLT with the ASCE and NLTH results: (a) V; (b) D.

was assigned to the weight factors (F_D, F_A, and F_V for D, A, and V, respectively), considering that all EDPs had the same importance. For the DBE level (life safety), the EDP ratios $\left(\frac{V_{avg}}{V_{lim}}; \frac{A_{avg}}{A_{lim}}; \frac{D_{avg}}{D_{lim}}\right)$ were found to be 0.43, 0.40, and 0.65, respectively. For the MCE level (collapse prevention), the values are 0.6, 0.650, and 0.52, respectively. Based on these conditions, the resulting life safety and collapse prevention global seismic assessment ratios, (G_{LS}) and (G_{CP}), were 0.51 and 0.41, respectively, which correspond to moderate and poor seismic performance classifications. This means that this model can perform moderately during the DBE level but performs poorly under the MCE level. This requires additional attention to the components that are sensitive to each EDP at the MCE level. For example, connections, interior wall partitions, and external curtain walls, which are sensitive to D, need to be designed for large drifts. However, suspended ceilings, which are sensitive to A, need to be designed to accommodate large A values during the MCE level.

For the mass-irregular 3-story model, the acceleration of heavy equipment fixation requires more attention. Therefore, F_A was assumed to be 0.8, whereas F_D and F_V were assumed to be 0.1. Based on these assumptions, the resulting life safety and collapse prevention global seismic assessment ratios, (G_{LS}) and (G_{CP}), were 0.36 and 0.12, respectively, which correspond to poor and not

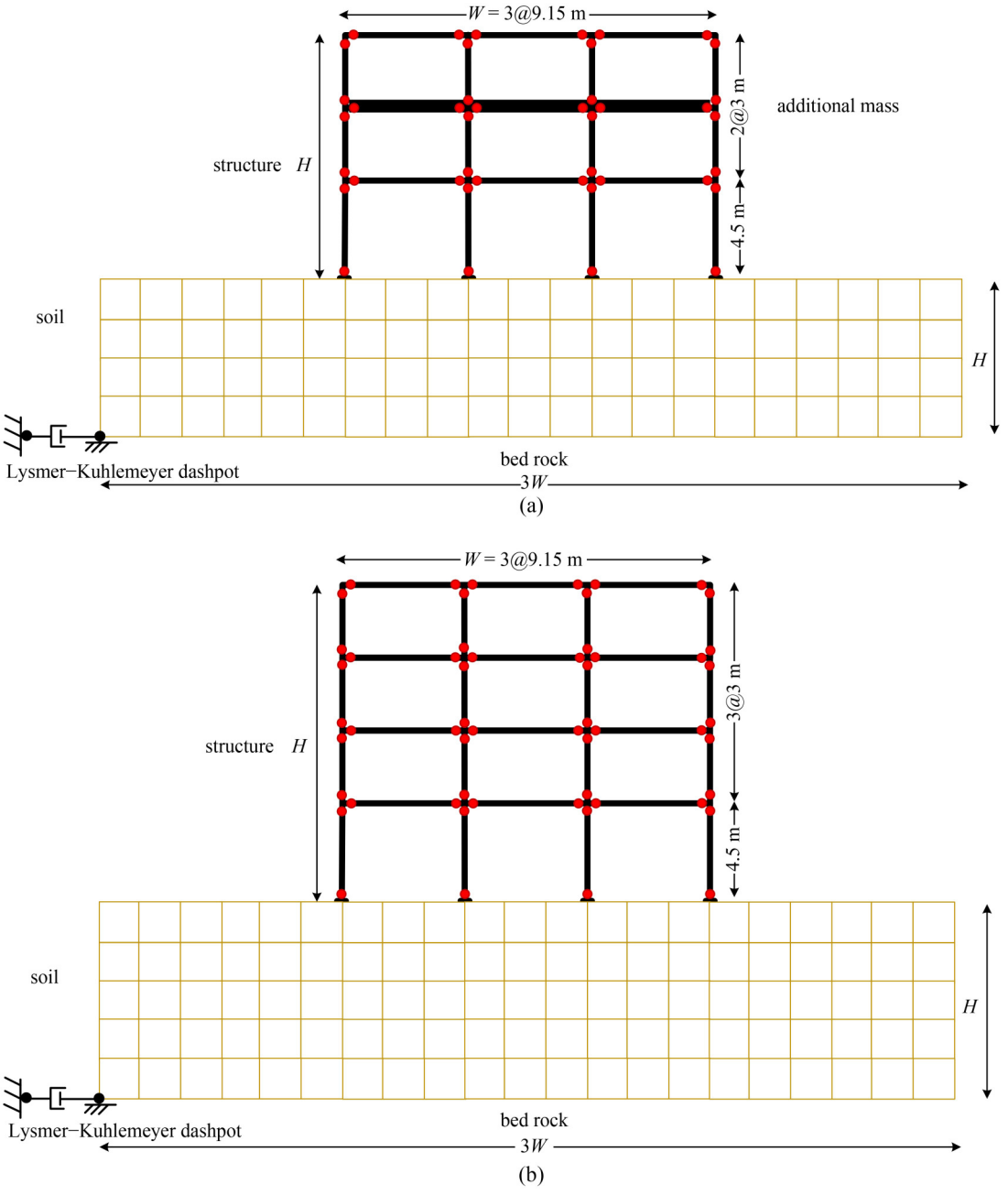

Fig. 15 Irregular framed structures: (a) 3-story with mass irregularity; (b) 4-story with stiffness irregularity.

acceptable seismic performance classifications. This requires fixation and the special arrangement of heavyweight equipment on the second floor, especially under the MCE level. Otherwise, the overall life-cycle cost of the building [65] will be excessively high in this case.

For the stiffness-irregular 4-story model, the importance goes to the drift, which necessitates F_D to be higher (assumed 0.8) than F_A and F_V (assumed 0.1 each). Based on that, the resulting G was 0.44, which makes the structure fall in the poor seismic performance classification. This may require reinforcement to decrease the drift by using bracings or additional damper devices.

4.6 Advantages of the proposed framework

The proposed framework has several advantages over the conventional methods. The main advantages of the proposed framework are summarized as follows.

1) A new global seismic assessment ratio that accounts for serviceability (A) and strength (D and V) aspects.

2) The consideration of multi-hazard levels in the seismic assessment.

3) The consideration of multiple limit states for assessment and design (e.g., life safety and collapse prevention).

4) The consideration of SSI parameters, and the

identification of the most important SSI parameters using a sensitivity analysis.

5) Less conservative results compared with ASCE methods by approximately 15%.

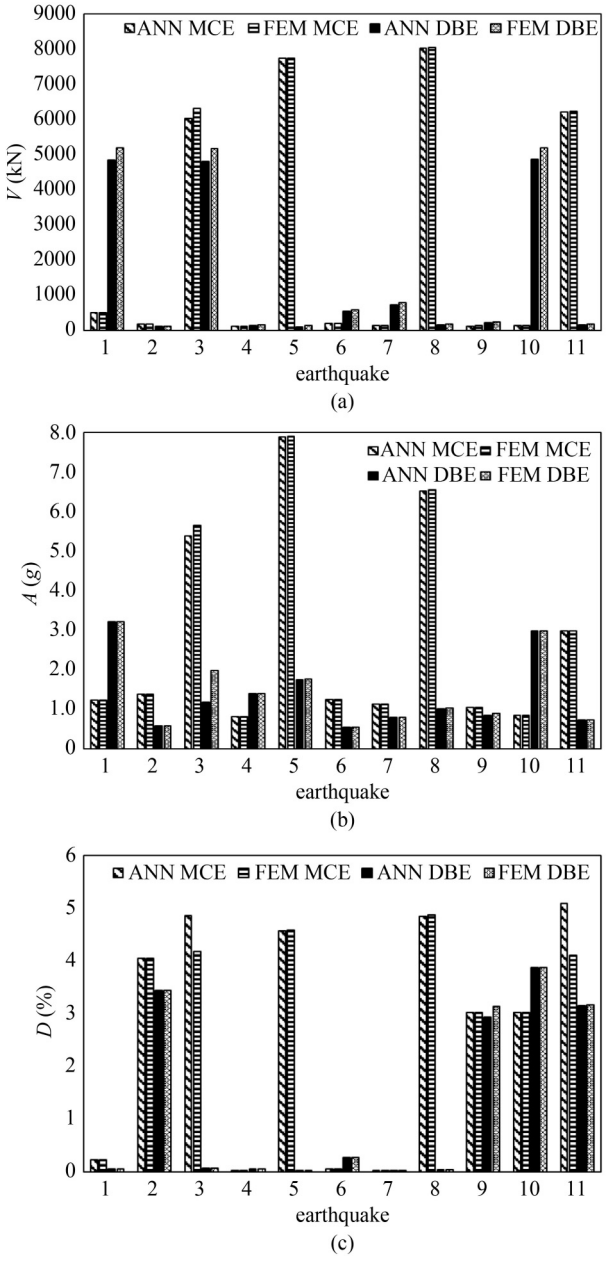

Fig. 16 Results of the mass irregular 3-story model obtained from NLTH analysis and the proposed MLT for the DBE and MCE level earthquakes: (a) V; (b) A; (c) D.

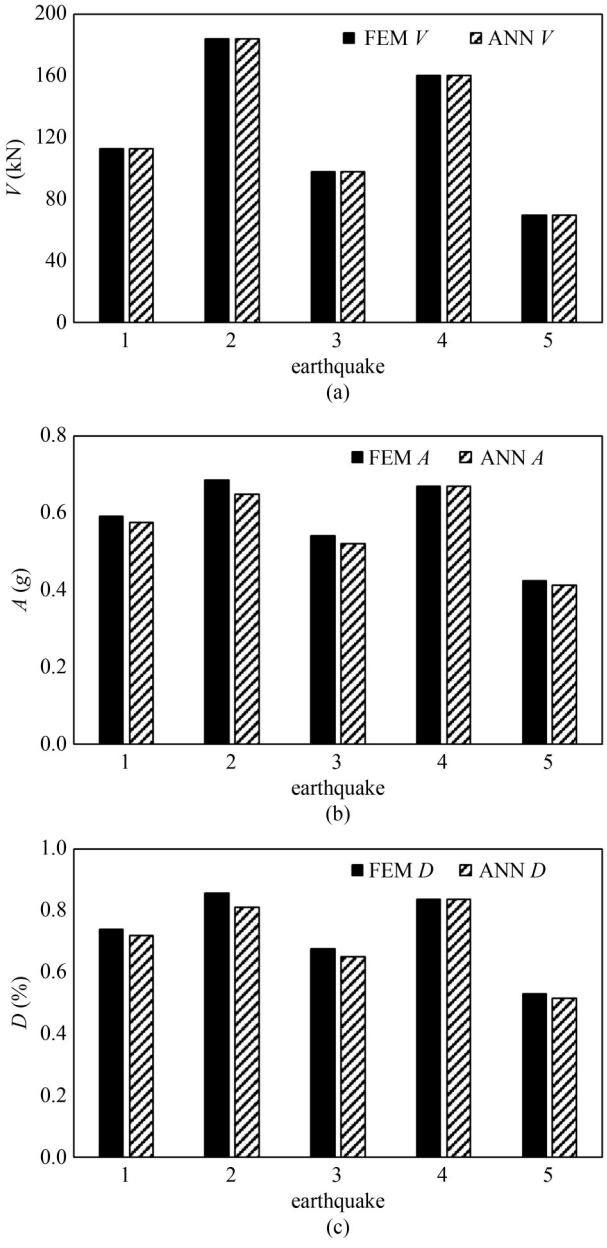

Fig. 17 Results of the stiffness irregular 4-story model obtained from NLTH analysis and the proposed MLT using 5 different earthquake records: (a) V; (b) A; (a) D.

Table 4 Global seismic assessment ratio (G)

model	limit state/EQ level	$(F_V)\frac{V_{avg}}{V_{lim}}$	$(F_A)\frac{A_{avg}}{A_{lim}}$	$(F_D)\frac{D_{avg}}{D_{lim}}$	global seismic assessment ratios (G)	seismic performance classifications
regular 3-story	life safety (DBE)	(1/3) 0.43	(1/3) 0.40	(1/3) 0.65	0.51	moderate
	collapse prevention (MCE)	(1/3) 0.6	(1/3) 0.65	(1/3) 0.52	0.41	poor
mass-irregular 3-story	life safety (DBE)	(0.1) 0.38	(0.8) 0.67	(0.1) 0.60	0.36	poor
	collapse prevention (MCE)	(0.1) 0.67	(0.8) 0.96	(0.1) 0.43	0.12	not acceptable
stiffness-irregular 4-story	selected	(0.1) 0.59	(0.1) 0.58	(0.8) 0.55	0.44	poor

6) Applicability to structures having limited irregularities, such as stiffness and mass irregularities.

7) Insight into the type of retrofit technique required for the structure based on DAV values.

8) If *D* is high, an increase in stiffness is required (e.g., adding bracings, dampers, etc.).

9) If *V* is high, an increase in strength is required for the important elements to remain elastic during excitation (e.g., bracing, column jacketing, and foundation retrofitting).

10) If *A* is high, attention is required for nonstructural elements and equipment that are sensitive to large *A* values.

11) Additional EDPs such as floor velocity, energy dissipation, and plastic hinge formation can be added easily.

12) Easy application to regional area surveys for seismic performance assessment of an inventory of buildings.

5 Conclusions

In the current study, an expert system framework for the seismic performance evaluation and classification of structures considering SSI was introduced. This framework consists of three main parts: dataset preparation, MLT selection, and seismic performance evaluation. The framework considers the serviceability and strength requirements with multiple limit states in the classification process. Several low- to mid-rise structures were used with dozens of natural earthquakes to conduct thousands of NLTH analyses. A sensitivity analysis was conducted on the output parameters to enhance the accuracy of the MLT. The framework was validated using an NLTH analysis and compared with conventional methods. Different structural irregularities were investigated to test the generalization potential of the framework. The main outcomes of this study are summarized as follows.

• The sensitivity analysis showed that *PGA* is the most important input parameter that affects the prediction of EDPs. This requires more attention from designers regarding this particular characteristic of an input earthquake.

• The best MLT accuracy can be achieved by using an ANN with two layers with 10 neurons per layer, the TANSIG activation function, and the LM training algorithm. In this case, the accuracy was 98.0%. This means that the framework can be reliably used as a design tool to quickly predict different EDPs. Moreover, the simplicity of the ANN makes it an easy to use tool for designers.

• The MLT-predicted results were in very good agreement with those of the NLTH results. The difference between the average results from both methods for the DBE and MCE levels was less than 4.0%. Based on these results, the framework can reduce the time required for long NLTH analyses while maintaining almost the same accuracy.

• The proposed framework provides a higher accuracy in predicting *V* and *D* compared with conventional ASCE methods. Additionally, the proposed framework with ANNs provides the most accurate results compared with ASCE methods. This is an interesting finding because it provides a reliable alternative to the ASCE method for predicting drifts while maintaining an accuracy similar to that of the NLTH method.

• The proposed framework shows high generalization potential for low- to mid-rise structures, and can be used for structures with limited irregularities and acceptable errors.

• The classification of the seismic performance of the investigated models could be accurately predicted by the proposed framework, considering the life safety and collapse prevention limit states and three different EDPs. The regular 3-story and mass-irregular 3-story models were classified as moderate and poor, respectively, for the DBE level; whereas they were classified as poor and not acceptable for the MCE level. The stuffiness-irregular 4-story model falls into the poor seismic performance classification. This finding is interesting because it provides a qualitative assessment of a building at different hazard levels, which is very important in the case of retrofitting or strengthening a deficient structure, as it will be useful in selecting a proper retrofitting scheme for the structure considering its seismic performance at different hazard levels.

Acknowledgements This study was supported by a National Research Foundation of Korea (NRF) grant funded by the Korean government (MSIT) (No. 2021R1A2C2006631).

References

1. Mayoral J M, Asimaki D, Tepalcapa S, Wood C, Roman-de la Sancha A, Hutchinson T, Franke K, Montalva G. Site effects in Mexico City basin: Past and present. Soil Dynamics and Earthquake Engineering, 2019, 121: 369−382
2. FEMA P-58-1. 2nd ed. Seismic Performance Assessment of Buildings—Volume 1—Methodology FEMA P-58-1. Washington, D.C.: Federal Emergency Management Agency, 2018
3. Bertero R D, Bertero V V. Performance-based seismic engineering: the need for a reliable conceptual comprehensive approach. Earthquake Engineering & Structural Dynamics, 2002, 31(3): 627−652
4. Lee S, Ha J, Zokhirova M, Moon H, Lee J. Background information of deep learning for structural engineering. Archives of Computational Methods in Engineering, 2018, 25(1): 121−129
5. Salehi H, Burgueno R. Emerging artificial intelligence methods in

structural engineering. Engineering Structures, 2018, 171: 170−189
6. Falcone R, Lima C, Martinelli E. Soft computing techniques in structural and earthquake engineering: A literature review. Engineering Structures, 2020, 207: 110269
7. Psyrras N K, Sextos A G. Build-X: Expert system for seismic analysis and assessment of 3D buildings using OpenSees. Advances in Engineering Software, 2018, 116: 23−35
8. Berrais A, Watson A S. Expert systems for seismic engineering: The state-of-the-art. Engineering Structures, 1993, 15(3): 146−154
9. Berrais A. A knowledge-based expert system for earthquake-resistant design of reinforced concrete buildings. Expert Systems with Applications, 2005, 28(3): 519−530
10. Sharma N, Dasgupta K, Dey A. Natural period of reinforced concrete building frames on pile foundation considering seismic soil-structure interaction effects. Structures, 2020, 27: 1594−1612
11. van Nguyen D, Kim D, Duy Nguyen D. Nonlinear seismic soil-structure interaction analysis of nuclear reactor building considering the effect of earthquake frequency content. Structures, 2020, 26: 901−914
12. Dao N D, Ryan K L. Soil-structure interaction and vertical-horizontal coupling effects in buildings isolated by friction bearings. Journal of Earthquake Engineering, 2020, 26: 2124−2147
13. Fatahi B, Tabatabaiefar H R, Samali B. Performance based assessment of dynamic soil-structure interaction effects on seismic response of building frames. In: Proceedings of Geo-Risk 2011: Risk Assessment and Management. Reston: ASCE, 2011, 344−351
14. Tang Y, Zhang J. Probabilistic seismic demand analysis of a slender RC shear wall considering soil-structure interaction effects. Engineering Structures, 2011, 33(1): 218−229
15. Reza Tabatabaiefar S H, Fatahi B, Samali B. Seismic behavior of building frames considering dynamic soil-structure interaction. International Journal of Geomechanics, 2013, 13(4): 409−420
16. Yang J, Lu Z, Li P. Large-scale shaking table test on tall buildings with viscous dampers considering pile-soil-structure interaction. Engineering Structures, 2020, 220: 110960
17. Liu S, Li P, Zhang W, Lu Z. Experimental study and numerical simulation on dynamic soil-structure interaction under earthquake excitations. Soil Dynamics and Earthquake Engineering, 2020, 138: 106333
18. Vaseghiamiri S, Mahsuli M, Ghannad M A, Zareian F. Probabilistic approach to account for soil structure interaction in seismic design of building structures. Journal of Structural Engineering, 2020, 146(9): 04020184
19. Khatibinia M, Javad Fadaee M, Salajegheh J, Salajegheh E. Seismic reliability assessment of RC structures including soil-structure interaction using wavelet weighted least squares support vector machine. Reliability Engineering & System Safety, 2013, 110: 22−33
20. Farfani H A, Behnamfar F, Fathollahi A. Dynamic analysis of soil-structure interaction using the neural networks and the support vector machines. Expert Systems with Applications, 2015, 42(22): 8971−8981
21. Mirhosseini R T. Seismic response of soil-structure interaction using the support vector regression. Structural Engineering and Mechanics, 2017, 63(1): 115−124
22. Siam A, Ezzeldin M, El-Dakhakhni W. Machine learning algorithms for structural performance classifications and predictions: Application to reinforced masonry shear walls. Structures, 2019, 22: 252−265
23. Estêvão J M C. Feasibility of using neural networks to obtain simplified capacity curves for seismic assessment. Buildings, 2018, 8(11): 151−161
24. Oh B K, Glisic B, Park S W, Park H S. Neural network-based seismic response prediction model for building structures using artificial earthquakes. Journal of Sound and Vibration, 2020, 468: 115109
25. Zhang Y, Gao Z, Wang X, Liu Q. Predicting the pore-pressure and temperature of fire-loaded concrete by a hybrid neural network. International Journal of Computational Methods, 2022, 468(3): 2142011
26. Zhang Y, Gao Z, Wang X, Liu Q. Image representations of numerical simulations for training neural networks. Computer Modeling in Engineering and Sciences, 134(2): 1−13
27. Noureldin M, Ali A, Nasab M S, Kim J. Optimum distribution of seismic energy dissipation devices using neural network and fuzzy inference system. Computer-Aided Civil and Infrastructure Engineering, 2021, 36(10): 1306−1321
28. Oh B K, Park Y, Park H S. Seismic response prediction method for building structures using convolutional neural network. Structural Control and Health Monitoring, 2020, 27(5): 1−10
29. ASCE 7-16. Minimum Design Loads for Buildings and Other Structures. Chicago: American Society of Civil Engineers, 2016
30. Khosravikia F, Mahsuli M, Ghannad M A. Comparative assessment of soil-structure interaction regulations of ASCE 7-16 and ASCE 7-10. In: Proceedings of Structures Congress 2018. Reston: ASCE, 2018
31. Khosravikia F, Mahsuli M, Ghannad M A. Soil-structure interaction in seismic design code: Risk-based evaluation. ASCE-ASME Journal of Risk and Uncertainty in Engineering Systems. Part A, Civil Engineering, 2018, 4(4): 04018033
32. Won J, Shin J. Machine learning-based approach for seismic damage prediction method of building structures considering soil-structure interaction. Sustainability (Basel), 2021, 13(8): 1−14
33. Xu J, Spencer B F Jr, Lu X, Chen X, Lu L. Optimization of structures subject to stochastic dynamic loading. Computer-Aided Civil and Infrastructure Engineering, 2017, 32(8): 657−673
34. Cimellaro G P, Reinhorn A M, Bruneau M. Seismic resilience of a hospital system. Structure and Infrastructure Engineering, 2010, 6(1−2): 127−144
35. Kim H S, Roschke P N. Fuzzy control of base-isolation system using multi-objective genetic algorithm. Computer-Aided Civil and Infrastructure Engineering, 2006, 21(6): 436−449
36. Kam W Y. Selective weakening and post-tensioning for the seismic retrofit of non-ductile RC frames. Dissertation for the Doctoral Degree. Christchurch: University of Canterbury, 2010, 532
37. Nour Eldin M, Naeem A, Kim J. Seismic retrofit of a structure using self-centering precast concrete frames with enlarged beam ends. Magazine of Concrete Research, 2020, 72(22): 1155−1170
38. Noureldin M, Memon S A, Gharagoz M, Kim J. Performance-based seismic retrofit of RC structures using concentric braced frames equipped with friction dampers and disc springs.

Engineering Structures, 2021, 243: 112555
39. Eldin M N, Dereje A J, Kim J. Seismic retrofit of framed buildings using self-centering PC frames. Journal of Structural Engineering, 2020, 146(10): 04020208
40. ASCE 41. Seismic Evaluation and Retrofit of Existing Buildings. Chicago: American Society of Civil Engineers, 2017
41. Nguyen-Le D H, Tao Q B, Nguyen V H, Abdel-Wahab M, Nguyen-Xuan H. A data-driven approach based on long short-term memory and hidden Markov model for crack propagation prediction. Engineering Fracture Mechanics, 2020, 235: 107085
42. Khatir S, Tiachacht S, Le Thanh C, Ghandourah E, Mirjalili S, Abdel Wahab M. An improved Artificial Neural Network using Arithmetic Optimization Algorithm for damage assessment in FGM composite plates. Composite Structures, 2021, 273: 114287
43. Wang S, Wang H, Zhou Y, Liu J, Dai P, Du X, Abdel Wahab M. Automatic laser profile recognition and fast tracking for structured light measurement using deep learning and template matching. Measurement, 2021, 169: 108362
44. Ho L V, Trinh T T, De Roeck G, Bui-Tien T, Nguyen-Ngoc L, Abdel Wahab M. An efficient stochastic-based coupled model for damage identification in plate structures. Engineering Failure Analysis, 2022, 131: 105866
45. Ho L V, Trinh T T, De Roeck G, Bui-Tien T, Nguyen-Ngoc L, Abdel Wahab M. A hybrid computational intelligence approach for structural damage detection using marine predator algorithm and feedforward neural networks. Computers & Structures, 2021, 252: 106568
46. OpenSees. Open System for Earthquake Engineering Simulation. Berkeley: Pacific Earthquake Engineering Research Center, 2011
47. MATLAB. Version R2020b. Reference Manual. 2020
48. FEMA P695. Quantification of Building Seismic Performance Factors. Washington, D.C.: MathWorks, 2009
49. Zhang Y, Zhuang X. Cracking elements: A self-propagating strong discontinuity embedded approach for quasi-brittle fracture. Finite Elements in Analysis and Design, 2018, 144: 84−100
50. Zhang Y, Mang H A. Global cracking elements: A novel tool for Galerkin-based approaches simulating quasi-brittle fracture. International Journal for Numerical Methods in Engineering, 2020, 121(11): 2462−2480
51. Zhang Y, Huang J, Yuan Y, Mang H A. Cracking elements method with a dissipation-based arc-length approach. Finite Elements in Analysis and Design, 2021, 195: 103573
52. Zhang Y, Gao Z, Li Y, Zhuang X. On the crack opening and energy dissipation in a continuum based disconnected crack model. Finite Elements in Analysis and Design, 2020, 170: 103333
53. Rabczuk T, Belytschko T. Cracking particles: A simplified meshfree method for arbitrary evolving cracks. International Journal for Numerical Methods in Engineering, 2004, 61(13): 2316−2343
54. Rabczuk T, Zi G, Bordas S, Nguyen-Xuan H. A simple and robust three-dimensional cracking-particle method without enrichment. Computer Methods in Applied Mechanics and Engineering, 2010, 199(37−40): 2437−2455
55. Zhang Y, Lackner R, Zeiml M, Mang H A. Strong discontinuity embedded approach with standard SOS formulation: Element formulation, energy-based crack-tracking strategy, and validations. Computer Methods in Applied Mechanics and Engineering, 2015, 287: 335−366
56. Lignos D G, Krawinkler H. Deterioration modeling of steel components in support of collapse prediction of steel moment frames under earthquake loading. Journal of Structural Engineering, 2011, 137(11): 1291−1302
57. Esmaeilzadeh Seylabi E, Jeong C, Taciroglu E. On numerical computation of impedance functions for rigid soil-structure interfaces embedded in heterogeneous half-spaces. Computers and Geotechnics, 2016, 72: 15−27
58. Feng S J, Zhang X K, Zheng Q T, Wang L. Simulation and mitigation analysis of ground vibrations induced by high-speed train with three dimensional FEM. Soil Dynamics and Earthquake Engineering, 2017, 94: 204−214
59. Bowles J E. Foundation Analysis and Design. 5th ed. New York: McGraw-Hill, 1996
60. Wen W, Zhang C, Zhai C. Rapid seismic response prediction of RC frames based on deep learning and limited building information. Engineering Structures, 2022, 267(15): 114638
61. Kim T, Kwon O S, Song J. Response prediction of nonlinear hysteretic systems by deep neural networks. Neural Networks, 2019, 111: 1−10
62. PEER. Pacific Earthquake Engineering Research Center: NGA Database. Berkeley: University of California, 2019
63. NIST GCR 12-917-21. Soil-structure Interaction for Building Structures. Berkeley: University of California, 2012
64. Li H, Chen C L P, Huang H P. Fuzzy Neural Intelligent Systems: Mathematical Foundation and the Applications in Engineering. Baca Raton: CRC Press, 2000
65. Noureldin M, Kim J. Parameterized seismic life-cycle cost evaluation method for building structures. Structure and Infrastructure Engineering, 2021, 17(3): 425−439